Finding eV-scale light relics with cosmological observables

Nicholas DePorzio,* Weishuang Linda Xu, Julian B. Muñoz, and Cora Dvorkin
Department of Physics, Harvard University, Cambridge, Massachusetts 02138, USA

(Received 23 June 2020; accepted 23 November 2020; published 4 January 2021)

Cosmological data provide a powerful tool in the search for physics beyond the Standard Model (SM). An interesting target are light relics, new degrees of freedom which decoupled from the SM while relativistic. Nearly massless relics contribute to the radiation energy budget, and are commonly parametrized as variations in the effective number $N_{\rm eff}$ of neutrino species. Additionally, relics with masses greater than 10^{-4} eV become nonrelativistic before today, and thus behave as matter instead of radiation. This leaves an imprint in the clustering of the large-scale structure of the Universe, as light relics have important streaming motions, mirroring the case of massive neutrinos. Here we forecast how well current and upcoming cosmological surveys can probe light massive relics. We consider minimal extensions to the SM by both fermionic and bosonic relic degrees of freedom. By combining current and upcoming cosmic-microwave-background and large-scale-structure surveys, we forecast the significance at which each light massive relic, with different masses and temperatures, can be detected. We find that a very large coverage of parameter space will be attainable by upcoming experiments, opening the possibility of exploring uncharted territory for new physics beyond the SM.

DOI: 10.1103/PhysRevD.103.023504

I. INTRODUCTION

The nature of the dark sector is one of the major puzzles of fundamental physics, integral to the understanding of our Universe across almost every epoch. Searches for the composition of the dark sector and, more broadly, of physics beyond the Standard Model (SM), take place at different energy scales, and use data ranging from particle colliders to astrophysical and cosmological surveys. The interactions of the dark sector with the SM are central to many of these searches. Yet, the small energies and interaction cross sections expected in many models often result in low experimental sensitivity to new physics. In contrast, by exploring the entropic effects of new dark-sector physics, cosmological data is in an exciting position to make robust discoveries.

Numerous extensions of the SM happen to posit the existence of light, feebly interacting particles, including axions and axionlike particles [1–4], dark photons [5–8], and light fermions [9–11]. One broad category are *light relics*, stable particles which were in thermal contact with the SM in the early Universe and decoupled while relativistic. Consequently, their cosmic abundance was frozen and survived until $z = 0$. The quintessential example within the SM are neutrinos, but they need not be the only light relics to populate our Universe. Different proposed new light relics include a fourth, sterile neutrino, whose existence is suggested by different anomalous experimental results [12–14] (see Ref. [15] for a recent review), as well as the gravitino, the supersymmetric partner of the graviton [16].

New relics that are sufficiently light will manifest as dark radiation, and can be searched for through their effect on the cosmic microwave background (CMB) anisotropies [17–19], typically parametrized by the effective number of neutrino species, $N_{\rm eff}$ (which is 3.045 in the standard cosmological model [20–22]). Massive relics can, on the other hand, become nonrelativistic at some point in cosmic history, and behave as other components of matter in the Universe thereafter. However, their decoupling while relativistic gives these relics significant streaming motion, which sets a scale below which they cannot cluster, thus altering the large-scale structure (LSS) of our Universe. This has allowed cosmology to set the leading constraints on neutrino mass, at $\Sigma m_\nu < 0.26$ eV (95% C.L.), assuming standard cosmology [23]. In this work we will search for new light—but massive—relics (LIMRs) using cosmological observables.

Cosmological data from near-future surveys are expected to provide exquisite measurements of the distribution of matter in our Universe. LIMRs that have become nonrelativistic before $z = 0$ (with masses $m_X \gtrsim 10^{-3}$ eV), will impact that distribution by behaving as hot dark matter [24–28]. In addition to the relic mass, two relevant parameters determine the relic abundance. The first is their number g_X of degrees of freedom. The second is their temperature $T_X^{(0)}$ today. Due to comoving-entropy conservation, any relic that was in equilibrium with the SM in the

*nicholasdeporzio@g.harvard.edu

early Universe ought to have $T_X^{(0)} \geq 0.91$ K. This minimum temperature gives rise to different values of $\Delta N_{\rm eff}$ for each type of relic [29]: 0.027 for scalars ($g_X = 1$), 0.047 for Weyl fermions ($g_X = 2$), 0.054 for massless gauge bosons ($g_X = 2$), and 0.095 for Dirac fermions ($g_X = 4$). In addition, relics with masses in the eV scale will become nonrelativistic before $z = 0$, leaving an imprint in the form of suppressed matter fluctuations. Here we forecast how well eV-scale LIMRs can be observed by joint CMB and LSS surveys.

This paper is structured as follows. In Sec. II we briefly review light relics and their effects on cosmological observables. In Sec. III we detail the datasets we consider, which we employ in Sec. IV to forecast constraints on LIMRs within the mass range 10^{-2}–10^{1} eV. We conclude in Sec. V.

II. LIGHT RELICS AND THEIR EFFECT ON COSMOLOGICAL OBSERVABLES

We begin with an overview of the physics of light relics and their effects on cosmological observables. A LIMR X is characterized by its present-day temperature $T_X^{(0)}$ and mass m_X, as well as its statistics, bosonic or fermionic, and its number g_X of degrees of freedom. The present-day temperature of a light relic (massive or not) is set by the time at which it decouples from the SM thermal bath, which is found as

$$T_X^{(0)} = \left(\frac{g_{*S}^{(0)}}{g_{*S}^{(\rm dec)}}\right)^{1/3} T_\gamma^{(0)}, \tag{1}$$

where $g_{*S}^{(0/\rm dec)}$ denotes the entropy degrees of freedom in the Universe today/when the relic decoupled, and $T_\gamma^{(0)} = 2.725$ K is the present-day temperature of the photon bath. In this way, the conservation of comoving entropy provides a minimal light relic temperature assuming the SM with no additional degrees of freedom (other than the relic),

$$T_X^{(0)} \gtrsim \left(\frac{3.91}{106.75}\right)^{1/3} T_\gamma^{(0)} \approx 0.91 \text{ K}, \tag{2}$$

where just after the electroweak phase transition we have $g_{*s}^{(\rm dec)} = 106.75$ encompasses all the known degrees of freedom of the Standard Model, and the present-day value of $g_{*s}^{(0)} = 3.91$ includes photons and decoupled, cooler neutrinos. As an example, the SM (active) neutrinos have $T_\nu^{(0)} = 1.95$ K, as they decoupled just prior to electron-positron annihilation where $g_{*s}^{(\rm dec,\nu)} = 10.75$. Note that the baryonic and cold-dark matter (CDM) contributions are negligible, given their exponentially suppressed abundance.

In contrast, light relics decoupled while relativistic, and so are cosmologically abundant, with number densities comparable to that of photons or neutrinos. For instance, a Weyl fermion decoupling as early as possible (with minimal present-day temperature 0.91 K) will have a number density today of 11 cm^{-3}, and a vector boson that decouples just before e^+e^- annihilation (with a temperature today of 1.95 K, as neutrinos) will have a present-day number density of 150 cm^{-3}. Thus, the contribution of light relics to the cosmic energy budget can be significant.

It is often enlightening to describe the cosmological effects of other relics in relation to those of neutrinos, given their common origin as light relics. As advanced in the introduction, relics in the early Universe (while $T_X \gg m_X$) behave as radiation, and their cosmological impact while relativistic can be encapsulated in the number of effective neutrinos, $N_{\rm eff}$, defined with respect to their contribution to the radiation energy density,

$$\begin{aligned}\rho_{\rm rad}(z) &= \frac{\pi^2}{30}\left(\sum_{\rm bosons} g_b T_b^4(z) + \frac{7}{8}\sum_{\rm fermions} g_f T_f^4(z)\right) \\ &\equiv \frac{\pi^2}{30}\left(2T_\gamma^4(z) + \frac{7}{4}N_{\rm eff}T_\nu^4(z)\right),\end{aligned} \tag{3}$$

where $T_{\gamma/\nu}(z)$ is the temperature of photons and neutrinos at redshift z, g_b/g_f are the degrees of freedom, and T_b/T_f are the temperatures of each boson/fermion, respectively.

Introducing an entropically significant light relic will generate a contribution to Eq. (3) of $(\pi^2/30)g_X T_X^4$ for bosonic species, or 7/8 times that for fermionic species. We can then describe any departure from the predicted value of $N_{\rm eff}^{\Lambda\rm CDM} = 3.045$ in the standard ΛCDM model by the quantity $\Delta N_{\rm eff}$, given by

$$\Delta N_{\rm eff} = c_1^\gamma \left(\frac{g_X}{g_\nu}\right)\left(\frac{T_X^{(0)}}{T_\nu^{(0)}}\right)^4, \tag{4}$$

in terms of the neutrino parameters $g_\nu = 2$ and $T_\nu^{(0)} = 1.95$ K. The factor $c_1 = 8/7$ accounts for the difference between the Bose-Einstein ($\gamma = 1$) and Fermi-Dirac ($\gamma = 0$) distributions.

This discussion is encapsulated in Fig. 1, showing the relation between the present-day relic temperature to the time of relic decoupling, and its corresponding contribution to $N_{\rm eff}$. Note that the present-day temperature of a relic for fixed decoupling epoch does not depend on particle species, but its contribution to radiation energy does.

Current limits on $\Delta N_{\rm eff}$ arise primarily from observables at two epochs. The first is recombination. Measurements of radiation at recombination are sensitive to relics lighter than ∼0.1 eV. The Planck 2018 analysis reports a measurement of $N_{\rm eff} = 2.99^{+0.34}_{-0.33}$ (TT + TE + EE + lowE + lensing + BAO) at 95% C.L. [23]. The proposed CMB-Stage 4 (CMB-S4) experiment is expected to refine this measurement to the $\sigma(N_{\rm eff}) = 0.03$ level [30]. The second is the Helium abundance, from where we can infer the number of relativistic species present during big bang

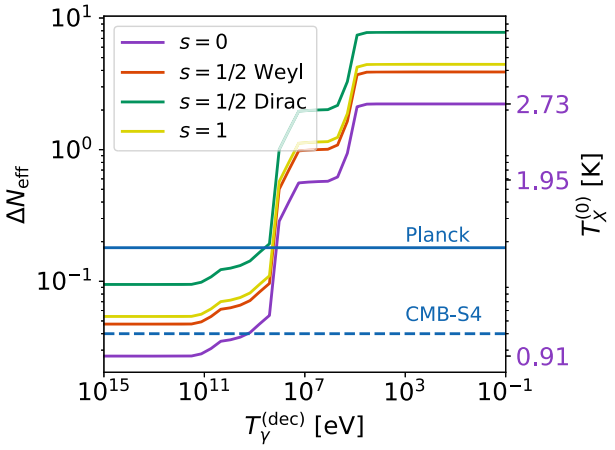

FIG. 1. Cosmic evolution of $\Delta N_{\rm eff}$ due to a light relic that decoupled when the Universe had a temperature $T_\gamma^{(\rm dec)}$. We assume four different types of relics with spin s, as described in the text, and show the 68% C.L. constraints achieved by Planck as a horizontal solid line, and the forecast by CMB-S4 in dashed lines. The right vertical axis shows what the temperature of the relic would be at $z = 0$, following the violet (lowest) curve plotted for $s = 0$. Note that these constraints only apply to relics with $m_X \approx 0.1$ eV or lighter.

nucleosynthesis (BBN). The 68% C.L. measurement during that era is $N_{\rm eff} = 2.85 \pm 0.28$ [31], which is valid for all relics lighter than $m_X \lesssim 10^6$ eV. Note that this does not affect dark matter (DM) produced via the freeze-in mechanism, as it can contribute negligibly to $N_{\rm eff}$ [32,33].

In this work we consider detection prospects for four types of LIMRs: scalars, vectors, and both Dirac and Weyl fermions. We study relics with eV-scale masses, 10^{-2} eV $\leq m_X \leq 10^1$ eV, such that they all behave as matter at $z = 0$, with the highest mass candidates constituting up to ~10% of DM abundance. Finally, we also consider a range of temperatures, bounded by $T_X^{(0)} \geq 0.91$ K from below. Our maximum temperature is informed by the constraint $\Delta N_{\rm eff} \leq 0.36$ from Planck, corresponding to a single additional species of Weyl fermion at $T_X^{(0)} \leq 1.5$ K. This bound could be further improved by combining with BBN measurements of, e.g., D/H ratios [34], Lyman-α forest flux power spectrum data [35,36], as well as baryon acoustic oscillations (BAO) and galaxy power spectrum measurements [37–39].

A. Effect on the LSS of the Universe

LIMRs can become non-relativistic at some point in cosmic history, and comprise a fraction of DM at $z = 0$. Unlike CDM, which is expected to compose the majority of the matter sector, LIMRs have significant thermal motions, even if nonrelativistic. Thus, these relics will stream away from structures below their free-streaming scale, which during matter domination is given by [40,41]

$$k_{\rm fs} = \frac{0.08}{\sqrt{1+z}} \left(\frac{m_X}{0.1\ \text{eV}}\right) \left(\frac{T_X^{(0)}}{T_\nu^{(0)}}\right)^{-1} h\,\text{Mpc}^{-1}. \quad (5)$$

Throughout this section we assume a Weyl fermionic relic, and we will relax this assumption later. This presents another way of searching for LIMRs: through their effect on the matter fluctuations. LIMRs produce a suppression in the matter power spectrum at scales smaller than $k_{\rm fs}$, which we discuss below. The size of this suppression depends on the present abundance of the LIMR, which (if nonrelativistic) is given by

$$\Omega_X h^2 = \frac{m_X}{93.14\ \text{eV}} \frac{g_X}{g_\nu} \left(\frac{T_X^{(0)}}{T_\nu^{(0)}}\right)^3. \quad (6)$$

From Eq. (6) we see that there is a maximum allowed particle mass, found by saturating the observed DM abundance $\Omega_{\rm cdm} h^2 = 0.12$ [23]. For a relic temperature $T_X^{(0)} \approx 1.5$ K, this is $m_X \approx 10$ eV. Additionally, in this work we are interested in the relics that become nonrelativistic before today. Thus, the mass range we will study encompasses

$$10^{-2}\ \text{eV} \leq m_X \leq 10^1\ \text{eV}. \quad (7)$$

LIMRs produce a suppression in matter fluctuations, similar to neutrinos, due to two reasons. The first is simply that the light relic does not cluster at small scales, and its fluctuation δ_X at small-scale roughly follows $\delta_X = (k/k_{\rm fs})^{-2}\delta_m$ with respect to the matter overdensity δ_m. The second is that the absence of relic fluctuations at small scales slows down the growth of CDM (and baryon) overdensities. Together, these two factors produce a suppression of roughly $(1 - 14 f_X)$ in the matter power spectrum [42], where f_X is the fraction of matter that is composed of the LIMR X. This suppression is less pronounced for relics that stay relativistic for longer, which yields the well-known result of $(1 - 8 f_\nu)$ for neutrinos comprising a fraction f_ν of matter, as neutrinos only become nonrelativistic during matter domination. These numbers are for illustration purposes only, and in all cases we find the full effect of LIMRs on the cosmological observables using the publicly available software CLASS [43]. Nevertheless, they provide intuition about the physical effect of such a relic. While the mechanism that produces the suppression is the same as for neutrino masses, the free-streaming scale $k_{\rm fs}$ for a LIMR is not fully determined by its mass (or abundance), as their temperature today is unknown. Relics that are still relativistic at $z = 0$ (with $m_X \lesssim 10^{-3}$ eV) will have never collapsed into structures and thus their observable effects can be fully included into $\Delta N_{\rm eff}$. In practice, this is the case for LIMRs with masses below ~0.1 eV, as we will show, so we will use our results for a 10^{-2} eV relic for lighter masses.

To study LIMRs, the relevant observables are the fluctuations of baryons and cold dark matter, as only those will gravitationally bind to form the visible structures we observe as galaxies, the relics being too light to cluster (see, however, Ref. [44]). The power spectrum of baryonic plus cold dark matter fluctuations is modeled by

$$P_{\rm cb}(k) = P_\zeta(k)(f_b T_b(k) + f_c T_c(k))^2, \tag{8}$$

where P_ζ is the primordial power spectrum, the transfer functions T_b and T_c are found using CLASS [43], and the fractional abundances are defined by

$$f_{b/c} \equiv \frac{\omega_{b/c}}{\omega_b + \omega_c}, \tag{9}$$

where ω_b and ω_c are the baryon and CDM abundances.

We show the suppression in $P_{\rm cb}$ in Fig. 2 (upper panel) for a fermion with $m_X = 0.02$ eV and $T_X = 0.91$ K, for degrees of freedom $g_X = 2$, 3, and 4. In all cases the high-k power is more suppressed, as expected. Increasing the abundance of the LIMR, by augmenting g_X, produces a more marked suppression, while keeping the shape fixed. Moreover, increasing the relic abundance produces wiggles at the BAO scale, as the LIMR both contributes as radiation at recombination and free streams—like neutrinos—changing the BAO phase [17].

The suppression of matter fluctuations produces a change in the biasing of galaxies, which has been calculated for both neutrinos and other relics [45–47], and accounted for in neutrino-mass forecasts in our companion paper [48]. This produces a growth in the galaxy power spectrum that partially compensates the relic-induced suppression. Here we account for this growth induced scale-dependent bias (GISDB) by multiplying the Lagrangian bias by a k-dependent factor

$$g(k) = R_L^{\Lambda\rm CDM}(k) R_L^X(k) R_L^\nu(k), \tag{10}$$

where the functions R_L^i account for different effects, following Ref. [46]. First, $R_L^{\Lambda\rm CDM}$ accounts for the steplike change in the growth rate of fluctuations before and after matter-radiation equality, parametrized as

$$R_L^{\Lambda\rm CDM}(k) = 1 + \Delta_{\Lambda\rm CDM} \tanh\left(\frac{\alpha k}{k_{\rm eq}}\right), \tag{11}$$

where $\Delta_{\Lambda\rm CDM} = 4.8 \times 10^{-3}$ and $\alpha = 4$ determine the amplitude and location of the step, given the scale $k_{\rm eq}$ of matter-radiation equality. The two other factors account for the effect of a LIMR on the matter power spectrum, also taken to be a steplike function

$$R_L^i(k) = 1 + \Delta_i \tanh\left(1 + \frac{\ln q_i(k)}{\Delta q}\right), \tag{12}$$

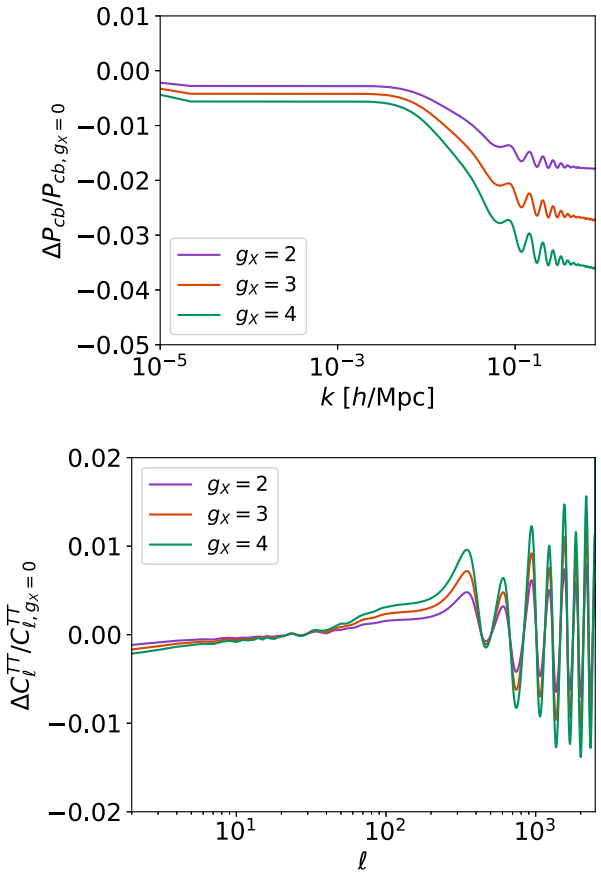

FIG. 2. Effect of introducing a fermion with degrees of freedom g_X, temperature $T_X = 0.91$ K, and mass $m_X = 0.02$ eV on the CDM + baryon power spectrum (upper panel) and the CMB temperature power spectrum (lower panel). Here all cosmological parameters are fixed when introducing the LIMR so the fraction of the matter or radiation energy occupied by the LIMR before and after its nonrelativistic transition will increase with its abundance. Since the LIMR energy density is not counted in the CDM plus baryon power spectrum, an increase in LIMR abundance will manifest as an overall suppression to P_{cb}. We note that an effective fractional number of degrees of freedom may be achieved as a result of out-of-equilibrium processes.

with an amplitude $\Delta_i = 0.6 f_i$ determined by the fraction f_i of matter composed of the relic i (X or ν), width $\Delta q = 1.6$, and where we have defined $q_i(k) \equiv 5k/k_{{\rm fs},i}$, given the free-streaming scale $k_{{\rm fs},i}$ of each LIMR.

B. Effect on the CMB

The CMB is sensitive to the presence of LIMRs in the Universe, through their mean energy density [49,50] and their perturbations [51,52]. Their additional energy density changes the expansion rate of the Universe, which in turn affects the CMB damping tail. Since matter-radiation equality is very well measured through the location of the first acoustic peak, this causes the power spectrum to be suppressed on short-wavelength modes. In addition to this effect, their perturbations cause a change in the amplitude

and a shift in the location of the CMB acoustic peaks (for a review of the phase shift in the acoustic peaks in the CMB, see Ref. [19]).

We show an example of the effect of a LIMR on the CMB in Fig. 2—again for a fermion with $m_X = 0.02$ eV and $T_X = 0.91$ K, for degrees of freedom $g_X = 2$, 3, and 4. The amplitude and phase shift of the BAO is clearly seen to increase with g_X.

C. Types of relic

Throughout this work we will study four major types of LIMRs, two fermionic and two bosonic, which we now describe.

In the fermionic category, the first type we study are the neutrinolike Weyl fermions, with nonzero mass, spin $s = 1/2$, and two degrees of freedom ($g_X = 2$). In addition to sterile neutrinos, an intriguing example is the gravitino, the supersymmetric partner of the graviton. While the gravitino has $s = 3/2$, only the longitudinal modes couple to the Standard Model and hence behaves equivalently to an $s = 1/2$ particle with $g_X = 2$. The gravitino is predicted in models of supersymmetric gravity to have a mass in the eV range [53,54], within the range relevant to our study. The second type we tackle are the related Dirac fermions, such as the axino [55], which simply have twice as many degrees of freedom ($g_X = 4$).

In the bosonic category we study two types of particles as well: first scalars, with only one degree of freedom ($g_X = 1$). A realization of this model could be a Goldstone boson, which can have naturally small masses. The second type are spin-1 vectors. We assume that they have a Stueckelberg mass, as it is technically natural [56] and avoids complications from Higgs mechanisms. While this relic will be nonrelativistic today, its longitudinal mode was decoupled in the early Universe (while it was relativistic), and thus only two of the three degrees of freedom were populated. Therefore, this relic has $g_X = 2$.

Instead of modifying the distribution function for each type of relic, we will take advantage of the fact that any relic, whether bosonic or fermionic, can be recast onto an equivalent Weyl relic (i.e., a neutrino with $g_W = 2$), with some temperature $T_W^{\rm eq}$ and mass $m_W^{\rm eq}$ [24,46]. Justification for this procedure is based on the results of other works which considered the significance of the distribution shapes for different species [46]. Assuming a relic of temperature T_X, with g_X degrees of freedom, the equivalent Weyl relic has

$$T_W^{\rm eq} = T_X (g_X/g_W)^{1/4} c_1^{\gamma/4}, \tag{13}$$

$$m_W^{\rm eq} = m_X (g_X/g_W)^{1/4} c_1^{\gamma/4} c_2^{\gamma}, \tag{14}$$

where we correct for the different distributions of these particles by setting $\gamma = 1$ for bosons (and $\gamma = 0$ for our base case of fermions as before), with constants $c_1 = 8/7$ [as in Eq. (4)] and $c_2 = 7/6$. Note that our normalization is slightly different from that found in Ref. [46], as there fermionic degrees of freedom contributed by 3/2.

III. METHODS

We now present our forecasting methods. In this first exploratory work we will follow a Fisher-matrix approach, in order to efficiently explore the 2D parameter space $(T_X^{(0)}, m_X)$ of possible LIMRs. We encourage the reader to visit Appendix A for a comparison against Markov chain Monte Carlo (MCMC) results. We will also cover different combinations of datasets. For the CMB, we will study the current Planck satellite [23] as well as the upcoming ground-based CMB-S4 [57]. On the galaxy-survey side we will consider the current BOSS [58], the ongoing DESI [59], and the upcoming Euclid [60] surveys.

A. Parameters

We are interested in forecasting how well different LIMRs with varied temperatures and masses can be detected. Therefore, a simple Fisher forecast of the relic mass and temperature, assuming a particular fiducial relic, is insufficient. Instead, we will find how well LIMRs of varying mass m_X and temperature $T_X^{(0)}$ can be observed by different experiments. The parameter we will forecast is g_X, the number of degrees of freedom of the LIMR.[1] Then, $g_X/\sigma(g_X)$ is a good proxy for the significance at which a LIMR of a particular m_X and $T_X^{(0)}$ can be detected.

In order to properly search for a LIMR we have to marginalize over the six ΛCDM parameters. These include the baryon and cold dark-matter abundances, ω_b and $\omega_{\rm cdm}$ (with fiducial values of $\omega_b = 0.02226$ and $\omega_{\rm cdm} = 0.1127$), the (reduced) Hubble constant $h = 0.701$, and the optical depth $\tau_{\rm reio} = 0.0598$ to reionization. The last two parameters are the amplitude A_s, and tilt n_s, of primordial fluctuations, with fiducial values of $A_s = 2.2321 \times 10^{-9}$ and $n_s = 0.967$. In addition, we marginalize over the effect of neutrino masses. We assume for our fiducial model the existence of three degenerate massive neutrinos, with $\sum m_\nu = 0.06$ eV, and we will report constraints both with and without marginalization over neutrino masses. Unless explicitly stated, no prior will be assumed for these parameters in the Fisher forecasts used to provide parameter constraints. For a discussion about the effect of the neutrino hierarchy see Refs. [48,61].

[1]We note that, while g_X appears to be a fixed quantity for a given relic, e.g., $g_X = 1$ for a scalar, changing g_X simply means altering the amount of relic particles (as both $\Delta N_{\rm eff} \propto g_X$ and $\Omega_X \propto g_X$) while keeping their thermal properties identical. That makes g_X a useful variable to forecast.

TABLE I. Forecasted number of target galaxies measurable by each survey: LRGs for BOSS, ELGs for DESI, and Hα emitters for Euclid per redshift per deg^2 at each redshift bin z, taken from Refs. [59,60,67].

z	0.05	0.15	0.25	0.35	0.45	0.55	0.65	0.75	0.85	0.95
$\frac{dN_{\rm LRG}}{dz\, d{\rm deg}^2}$ [BOSS]	8	50	125	222	332	447	208	30	0	0
$\frac{dN_{\rm ELG}}{dz\, d{\rm deg}^2}$ [DESI]	0	0	0	0	0	0	309	2269	1923	2094
$\frac{dN_{H\alpha}}{dz\, d{\rm deg}^2}$ [Euclid]	0	0	0	0	0	0	2434	4364	4728	4825
z	1.05	1.15	1.25	1.35	1.45	1.55	1.65	1.75	1.85	1.95
$\frac{dN_{\rm LRG}}{dz\, d{\rm deg}^2}$ [BOSS]	0	0	0	0	0	0	0	0	0	0
$\frac{dN_{\rm ELG}}{dz\, d{\rm deg}^2}$ [DESI]	1441	1353	1337	523	466	329	126	0	0	0
$\frac{dN_{H\alpha}}{dz\, d{\rm deg}^2}$ [Euclid]	4728	4507	4269	3720	3104	2308	1514	1474	893	497

B. CMB experiments

We will model both Planck and CMB-S4 as having a single effective observing frequency, to avoid marginalizing over foregrounds. For Planck we will use CMB temperature (T) and E-mode polarization data, covering the range $\ell = [2-2500]$. We take noises of $\Delta_T = 43\ \mu$K-arcmin and $\Delta_E = 81\ \mu$K-arcmin, with a $\theta_{\rm FWHM} = 5$ arcmin angular resolution. This well approximates the (more complex) Planck data likelihood.

For CMB-S4 we take $\Delta_T = 1\ \mu$K-arcmin, and $\Delta_E = \sqrt{2}\Delta_T$, with an angular resolution of $\theta_{\rm FWHM} = 3$ arcmin. Additionally, we include lensing data, where we perform iterative delensing of B modes to lower the noise, as in Refs. [62,63]. All modes cover the range $\ell = [30-5000]$, except for the TT autocorrelation, where we do not go beyond $\ell = 3000$ to avoid foreground contamination [30]. We add a Gaussian prior on the optical depth of reionization of $\sigma(\tau_{\rm reio}) = 0.01$, instead of the $\ell < 30$ modes in this case. This follows the prescription in the CMB-S4 science book [30], as well as our companion paper [48], and is the sensitivity reported from the Planck 2018 results. As such, it serves as a conservative estimate for futuristic surveys, such as CMB-S4 [23].

The CMB data will perform two main roles. First, it will very precisely measure the standard cosmological parameters, breaking many degeneracies in the LSS data. Second, the CMB is sensitive to the effects of a LIMR both during recombination and in the matter fluctuations at lower redshifts, through the weak lensing information.

C. Galaxy surveys

For the LSS data we will consider three surveys, all of them spectroscopic. We leave for future work studying the promise of photometric surveys, such as the Vera Rubin Observatory [64], and weak-lensing surveys, such as the Dark Energy Survey [65].

We take the luminous red galaxy (LRG) sample of the Sloan Digital Sky Survey Baryon Oscillation Spectroscopic Survey (BOSS) [58], which will serve as an indication of the power of current data. To showcase the promise of upcoming surveys we study the emission-line galaxy (ELG) sample of the Dark Energy Spectroscopic Instrument (DESI) [59], and the more futuristic Hα emitters of Euclid [60]. We restrict our analysis to a single tracer, the most populous for each survey, though more optimistic results are expected for multitracer approaches [66]. The noise per redshift bin for each sample is reported in Table I. We assume sky coverages of 10 000 deg^2 for BOSS, 14 000 deg^2 for DESI, and 15 000 deg^2 for Euclid.

As each of these surveys contain distinct tracers, the bias description of each will be somewhat different as well. Here we follow a simple approach, and parametrize the linear Eulerian bias as

$$b_1(k,z) = [1 + b_L(k,z) + \alpha_{k2}k^2], \tag{15}$$

where the α_k term (with a fiducial value of 1 Mpc^2) accounts for nonlinearities in the bias [68]. We emphasize that we do not include the clustering of light relics in this description. We also note that while cold dark matter and baryons may demonstrate different clustering behaviors at small scales, we do not consider such scales in this work and so do not include corrections to the bias that would differentiate the baryon and cold dark matter clustering fields. An additional scale-dependence comes from the aforementioned GISDB effect, which enters in the Lagrangian bias,

$$b_L(k,z) = [b_0(z) - 1]g(k), \tag{16}$$

where $g(k)$ is as defined in Eq. (10). The redshift evolution of the bias is encapsulated in the term $b_0(z)$, which is chosen such that the scale-independent (i.e., $k \to 0$) behavior of the Eulerian bias matches with suggestions made elsewhere in the literature [46]. For the ELGs in DESI we match to

$$b_0(z) = \frac{\beta_0}{D(z)}, \tag{17}$$

where $D(z)$ is the growth factor and $\beta_0 = 1$ [59]; whereas for the tracers in BOSS and Euclid we take

$$b_0(z) = \beta_0(1+z)^{0.5\beta_1}, \tag{18}$$

with fiducials $\beta_0 = 1.7$ and $\beta_1 = 1$ as in Ref. [69]. We marginalize over the nuisance parameters β_0, α_{k2}, as well as β_1 for BOSS and Euclid. We note that a full analysis of the data might require marginalization over the amplitude of the bias at each redshift bin independently, which would however lead to a loss in constraining power.

D. Fisher matrix

We will obtain forecasted constraints using the Fisher-matrix formalism [70–72]. For the CMB we follow the approach of Refs. [73,74]. For the galaxy observables we detail below how we construct our Fisher matrix.

As described in Sec. II, LIMRs suppress the clustering of matter in our Universe, and as a consequence, that of biased tracers of matter, such as galaxies. We take into account several effects to convert from matter to galaxy fluctuations. First, there are redshift-space distortions (RSD), induced by the gravitational infall into, and peculiar velocities of galaxies [75,76]. We write the galaxy power spectrum as

$$P_g(k,\mu) = \mathcal{R}(k,\mu)\mathcal{F}(k,\mu)P_{\rm cb}(k), \tag{19}$$

in terms of the power spectrum $P_{\rm cb}(k)$ of CDM + baryon fluctuations, where the two prefactors $\mathcal{R}$ and $\mathcal{F}$ account for the RSD and the finger-of-god (FOG) effect, both of which make P_g anisotropic, as they depend on $\mu = \hat{k}\cdot\hat{n}$, the line-of-sight angle.

We model the linear RSD term simply as

$$\mathcal{R}(k,\mu) = [b_1(k) + f\mu^2]^2, \tag{20}$$

where b_1 is the linear Eulerian bias, as described above, and $f \equiv d\ln D/d\ln a$ is the logarithmic derivative of the growth factor D, which can be well approximated by [77]

$$f(z) = \left(\frac{\Omega_{\rm cb}(1+z)^3}{\Omega_{\rm cb}(1+z)^3 + \Omega_\Lambda}\right)^\gamma, \tag{21}$$

with $\gamma = 0.55$. The nonlinear FOG effect is included in the term

$$\mathcal{F}(k,\mu) = \exp\left[-k^2\mu^2\sigma_v^2/H^2\right], \tag{22}$$

with $\sigma_v = (1+z)\sqrt{c^2\sigma_z^2 + \sigma_{\rm FOG}^2/2}$, where $\sigma_{\rm FOG} = \sigma_{\rm FOG}^{(0)}\sqrt{1+z}$, with $\sigma_{\rm FOG}^{(0)} \equiv 250\ {\rm km\,s^{-1}}$ [78] as the intrinsic velocity dispersion of galaxies, and we take a spectroscopic redshift error $\sigma_z \equiv 0.001c$ [59], which corresponds to the DESI precision requirement at $z = 1$.

In addition, we include the Alcock-Paczynski (AP) effect [79–81], which accounts for changes in the observed k and μ and the comoving volumes from assuming different cosmologies. For that, we write the observed galaxy power spectrum as [82]

$$\tilde{P}_g(k',\mu') = P_g(k,\mu)\left(\frac{H_{\rm true}}{H_{\rm fid}}\right)\left(\frac{D_{A,\rm fid}}{D_{A,\rm true}}\right)^2, \tag{23}$$

where the subscript "fid" refers to fiducial, and the "true" wave number k' and angle μ' are given by

$$k' = k\left[(1-\mu^2)\frac{D_{A,\rm fid}^2(z)}{D_{A,\rm true}^2(z)} + \mu^2\frac{H_{\rm true}^2(z)}{H_{\rm fid}^2(z)}\right]^{1/2}, \tag{24}$$

$$\mu' = \mu\frac{k}{k'}\frac{H_{\rm true}(z)}{H_{\rm fid}(z)}. \tag{25}$$

Properly accounting for the AP effect, thus, implies evaluating the entire galaxy power spectrum at different wave numbers for each cosmological-parameter change. That can be computationally consuming, so instead we will perform a simpler step that is accurate to first order in derivatives (as any further is not captured by Fisher). Therefore, we can write

$$\frac{\partial\tilde{P}_g(k',\mu')}{\partial\theta_i} = \frac{\partial P_g(k,\mu)}{\partial\theta_i} + \mathcal{C}_i(k), \tag{26}$$

for each parameter θ_i, where

$$\mathcal{C}_i(k) = \frac{\partial P_g}{\partial k}\frac{dk}{d\theta_i} + \frac{\partial P_g}{\partial\mu}\frac{d\mu}{d\theta_i}, \tag{27}$$

accounts for the AP correction to linear order, with the derivatives of k and μ computed from Eq. (25).

The Fisher element for parameters θ_i, θ_j is then calculated as [67]

$$F_{ij} = \sum_z \int k^2{\rm d}k \int {\rm d}\mu \frac{V(z)}{2(2\pi)^2}\left(\frac{\bar{n}\tilde{P}_g}{\bar{n}\tilde{P}_g + 1}\right)^2 \times \left(\frac{\partial\log\tilde{P}_g}{\partial\theta_i}\right)\left(\frac{\partial\log\tilde{P}_g}{\partial\theta_j}\right), \tag{28}$$

where $V(z)$ is the comoving volume for each redshift bin summed over, and $\bar{n}(z)$ is the comoving number density of tracers, given by $\bar{n}(z) = \Delta z f_{\rm sky}V^{-1}(z)dN/(dz\ d{\rm deg}^2)$, where the last factor is reported for each survey in Table I. The integral over μ goes from -1 to 1, and over wave numbers from $k_{\rm min} = \pi V(z)^{-1/3}$ to $k_{\rm max} = 0.2\ h\,{\rm Mpc}^{-1}$, which is mildly in the nonlinear regime [83]. While at

higher z the fluctuations are smaller and, thus, we could reach higher $k_{\rm max}$ while linear, the biasing of galaxies becomes more complex, so we fix $k_{\rm max}$ for all z. We expect that non-Gaussianities in the likelihood will affect constraints on cosmological parameters, but we do not model those effects in this work [84].

IV. RESULTS

In this section we discuss our cosmological constraints for a LIMR. We will perform two parallel analyses. First, we will show the reach of different combinations of datasets by forecasting $\sigma(g_X)$ for a Weyl (neutrinolike) relic of different masses and temperatures, covering the entire range of interest. Then, we will focus on the minimal case (that with $T_X^{(0)} = 0.91$ K) for the four relic types we consider, and find more precisely above which mass m_X they can be ruled out.

A. Full parameter space

We will start with a Weyl relic, and cover a broad range of cases, where in each case we will assume that there exists a LIMR in our Universe with mass m_X and temperature today $T_X^{(0)}$, and forecast how well g_X can be measured as a measure of how significant a detection would be.

We scan through a range of LIMR masses m_X from 10^{-2} eV, as all lighter relics behave identically, up to $\sim$10 eV, where the relic abundance overcomes that of all DM. As for their temperature, we cover $T_X^{(0)} = [0.91 - 1.50]$ K, where the lower limit is as found in Sec. II, and the upper limit saturates the current 95% C.L. Planck + BOSS DR12 BAO limit on $N_{\rm eff}$ [23].

First, as a test, we forecast the errors on $N_{\rm eff}$ by looking at our lightest relic ($m_X = 0.01$ eV) as a proxy of the massless case, and translating the forecasted error $\sigma(g_X)$ in the degrees of freedom into

$$\sigma(N_{\rm eff}) = \frac{\sigma(g_X)}{g_\nu}\left(\frac{T_X^{(0)}}{T_\nu^{(0)}}\right)^4. \tag{29}$$

For reference, we have confirmed that assuming lower values of m_X result in the same forecasts for $N_{\rm eff}$. This result is largely independent of the chosen $T_X^{(0)}$, so we will show forecasts for a Weyl fermion with $T_X^{(0)} = 0.91$ K.

Beginning with the CMB, the Planck-only forecast gives $\sigma(g_X) = 8.11$ corresponding to $\sigma(N_{\rm eff}) = 0.19$ which is in agreement with the Planck value of $\sigma(N_{\rm eff})$ in nonphoton radiation density when allowing extra relativistic degrees of freedom Ref. [23]. Likewise, the CMB-S4-only forecast yields $\sigma(N_{\rm eff}) = 0.040$. This is to be compared with the value of $\sigma(N_{\rm eff}) = 0.035$ reported in Ref. [30] for the same combination of resolution and sensitivity. The $\sim$10% difference is due to the delensing of T and E modes [19,85] that is performed in Ref. [30] but not in our forecasts. This is because we are chiefly interested in more massive relics, for which the phase shift is not the main cosmological signature.

TABLE II. Forecasted 1σ errors on $N_{\rm eff}$ from different combinations of experiments. Numbers in parenthesis assume fixed total neutrino mass, whereas the rest are marginalized over neutrino masses.

$\sigma(N_{\rm eff})$	CMB Only	BOSS	DESI	Euclid
LSS Only		0.92 (0.84)	0.29 (0.25)	0.20 (0.13)
Planck	0.19 (0.19)	0.14 (0.08)	0.06 (0.04)	0.06 (0.04)
CMB-S4	0.04 (0.04)	0.04 (0.03)	0.03 (0.02)	0.02 (0.02)

In both cases, as well as the ones below, we account for a noted degeneracy with Σm_ν by marginalizing over the neutrino mass in our forecasts. Adding LSS data only improves these results, as we show in Table II. In particular, we find that adding BOSS to Planck gives $\sigma(N_{\rm eff}) = 0.14$; substituting DESI for BOSS yields $\sigma(N_{\rm eff}) = 0.06$. Looking to the future, Euclid and CMB-S4 will lower this constraint to $\sigma(N_{\rm eff}) = 0.02$.

We now move to nonzero masses, and provide marginalized posteriors from forecasts for a 0.91 K (minimum temperature) Weyl relic at different masses in Fig. 3. We only show the 2D contours between g_X and other cosmological parameters; for the full triangle plots at fixed mass $m_X = 0.01$ eV, see Appendix C. The combination of information from the CMB and LSS can be seen to significantly improve constraints by breaking parameter degeneracies present in the individual datasets. Interestingly, the degeneracy directions change with LIMR mass. As an example, the degeneracy line for g_X and $\omega_{\rm cdm}$ for CMB data changes direction as the LIMR becomes more massive, and starts behaving as matter instead of radiation at recombination. The LSS degeneracy line, however, stays relatively stable, improving the CMB result by different amount at each mass.

The result described above indicates that combining CMB and LSS information is critical for an optimal constraint of LIMRs. We confirm this in Fig. 4, where we show the forecasted error in g_X for CMB and LSS data on their own, as well as together, which dramatically improves the constraints. For the rest of this work we will consider different combinations of CMB and LSS surveys together.

We now forecast to which level of significance different LIMR can be constrained, under three different survey combinations. The first is what would be realizable by current data, where we assume galaxy data from BOSS and Planck for the CMB. We show the forecasted $\sigma(g_X)$ in Fig. 5, which clearly shows that LIMRs with larger $T_X^{(0)}$ and m_X are more readily observable. However, to observe (or rule out) a LIMR at 3σ it has to be relatively heavy ($m_X \gtrsim$ few eV), as we will see below. Note that in this figure we show results for $T_X^{(0)} < 0.91$ K, as for instance a scalar

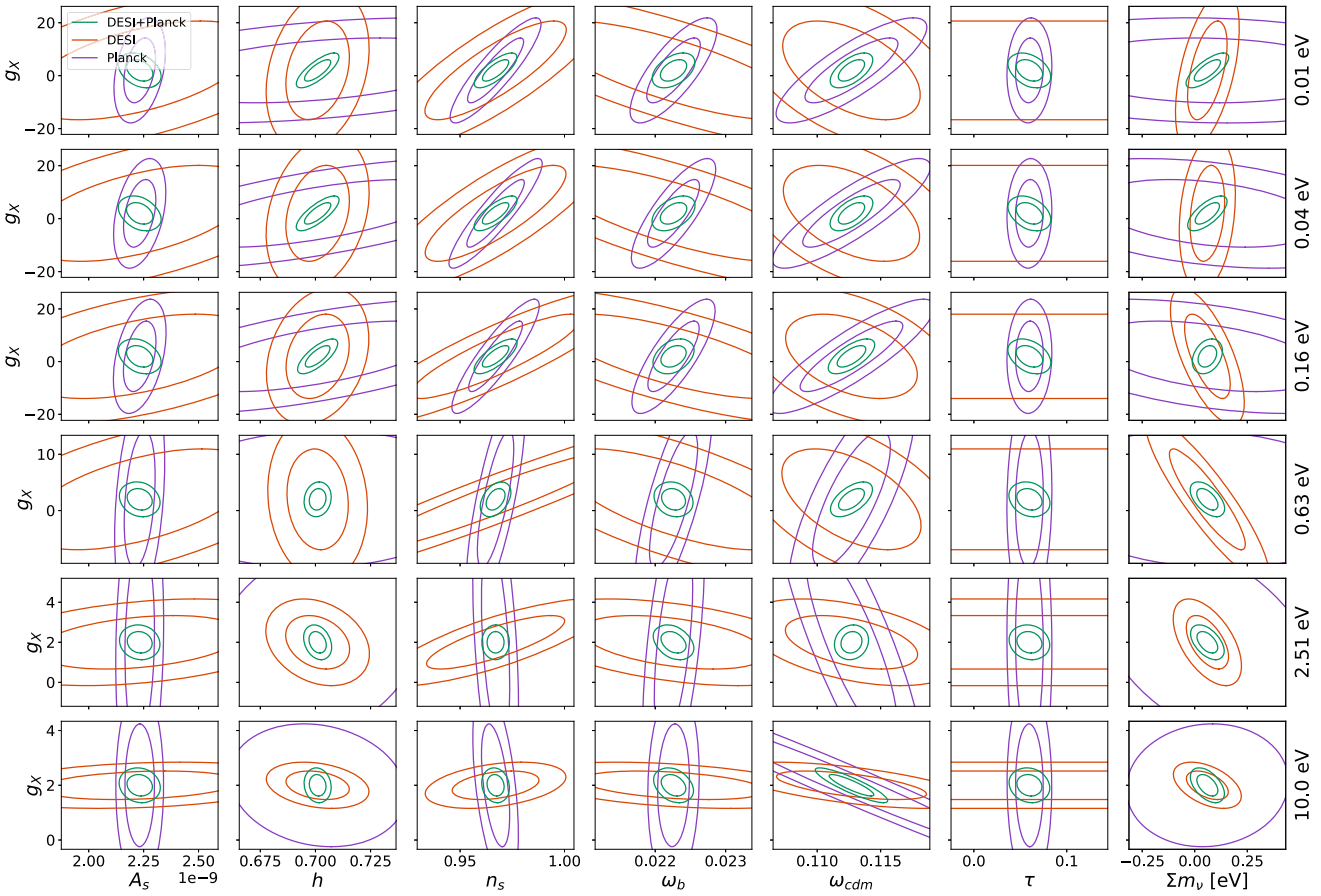

FIG. 3. 68% C.L. and 95% C.L. projected confidence ellipses for each of the parameters we marginalize over, as well as the LIMR number g_X of degrees of freedom, for DESI (red), Planck (purple), and their combination (green). Each row has a different fiducial relic mass, denoted on the right, all with an assumed temperature $T_X^{(0)} = 0.91$ K at $z = 0$. Note that we also marginalize over the unknown neutrino mass, which loosens our constraints by as much as 143% for LSS-only information, 64% for CMB-only information, and 81% for combined LSS and CMB information.

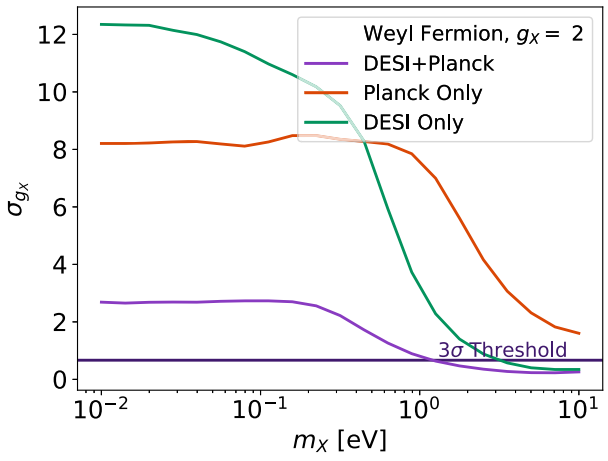

FIG. 4. Improvement of Weyl relic measurements by addition of LSS data with DESI and Planck constraints. The relic is fixed at its minimum possible temperature, $T_X^{(0)} = 0.91$ K. As shown, the joint constraints are much stronger than the LSS or CMB alone.

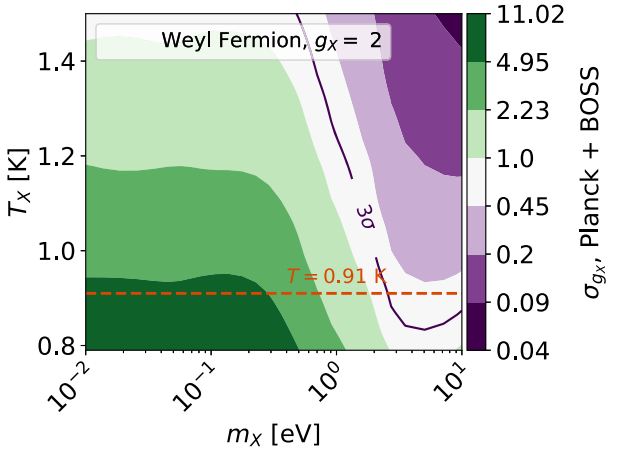

FIG. 5. Forecasted errors on g_X for a Weyl (neutrinolike) relic of different fiducial masses and temperatures, in all cases with fiducial $g_X = 2$, assuming BOSS + Planck data. The region of parameter space measurable at the 3σ-level lays rightward of the purple solid line, and the dashed red line shows the minimum temperature expected for a relic.

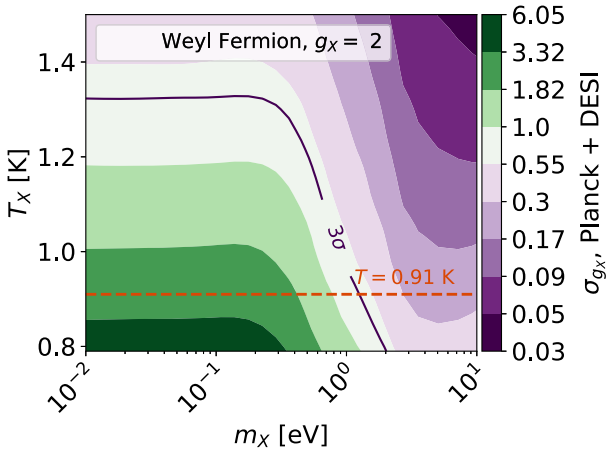

FIG. 6. Same as Fig. 5 for DESI + Planck.

at that minimum temperature would be equivalent to a Weyl fermion with $T_X^{(0)} = 0.79$ K, as we will discuss below.

The second case we consider is the near-future one, where we add DESI data to Planck. We show the forecasted constraints on g_X for this combination in Fig. 6, which are clearly improved with respect to the results shown in Fig. 5. In this case one can rule out relics of any mass with $T_X^{(0)} = 1.4$ K at 3σ. More interestingly, we see that masses above 1 eV would be ruled out, even for the lowest possible relic temperature of $T_X^{(0)} = 0.91$ K.

The final case we consider is more futuristic, and adds CMB-S4 data to DESI. We show the results in Fig. 7, which further improves the prospects for detecting light relics. In this case even relics at low temperatures can be ruled out at 3σ confidence for masses above 0.78 eV, whereas minimum-temperature massless Weyl relics can only be found at 0.5σ confidence.

B. Minimum temperature

While the figures discussed above covered a broad range of temperatures and masses, they all assumed a Weyl relic.

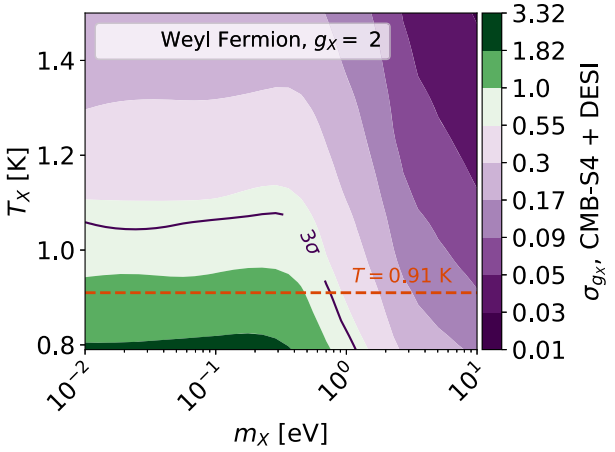

FIG. 7. Same as Fig. 5 for DESI + CMB-S4.

TABLE III. Minimum mass at which a LIMR (scalar boson, Weyl fermion, vector boson or Dirac fermion, from top to bottom) can be observed or ruled out at 3σ significance. Also reported in parentheses is the result with fixed $\sum m_\nu$ (to its fiducial value). A "$\cdots$" sign corresponds to no masses within the 3σ constraint. "**All**" corresponds to all LIMR masses analyzed being within the 3σ constraint.

	CMB Only	BOSS	DESI	Euclid
		Scalar m_X[eV]		
LSS Only		$\cdots$ ($\cdots$)	4.98 (4.54)	3.24 (3.22)
Planck	$\cdots$ ($\cdots$)	$\cdots$ ($\cdots$)	1.96 (1.61)	1.31 (1.16)
CMB-S4	1.48 (1.44)	1.41 (1.31)	1.14 (1.06)	0.93 (0.87)
		Weyl Fermion m_X[eV]		
LSS Only		$\cdots$ ($\cdots$)	3.13 (2.78)	2.42 (2.41)
Planck	$\cdots$ ($\cdots$)	2.85 (2.47)	1.20 (1.00)	0.87 (0.78)
CMB-S4	1.03 (1.02)	0.98 (0.91)	0.78 (0.71)	0.63 (0.59)
		Vector m_X[eV]		
LSS Only		$\cdots$ ($\cdots$)	2.41 (2.08)	1.88 (1.88)
Planck	$\cdots$ ($\cdots$)	2.05 (1.79)	0.90 (0.75)	0.65 (0.60)
CMB-S4	0.81 (0.78)	0.75 (0.70)	0.58 (0.54)	0.47 (0.44)
		Dirac Fermion m_X[eV]		
LSS Only		4.06 (3.72)	1.82 (1.36)	1.50 (1.50)
Planck	$\cdots$ ($\cdots$)	1.30 (1.12)	0.61 (0.52)	0.45 (0.43)
CMB-S4	0.56 (0.55)	0.51 (0.48)	**All** (**All**)	**All** (**All**)

Here we extend our results to other types of relics, focusing on the minimum temperature of $T_X^{(0)} = 0.91$ K, corresponding to the earliest decoupling from the SM plasma. We divide our results into fermionic and bosonic relics. The cumulative results of our forecast for each type of particle are tabulated in Table III.

1. Fermionic relics

We start with a massive Weyl fermion with $T_X^{(0)} = 0.91$ K, for which we show our forecasts on $\sigma(g_X)$ for various combinations of galaxy surveys and CMB experiments in Fig. 8(a), with a finer mass resolution than the results above. We report the minimum relic masses that are observable at 3σ significance, both with (and without) marginalizing over the neutrino masses, as a test of how degenerate LIMRs are with the total neutrino mass. The combination of presently available Planck and BOSS datasets are forecasted to observe or rule out LIMRs above 2.85 (2.47) eV at 3σ significance. For Planck and DESI, this is lowered to LIMRs with masses above 1.20 (1.00) eV. This result should motivate an analysis using presently available datasets. For the futuristic combination of CMB-S4 and Euclid datasets, we show that LIMR masses above 0.63 (0.59) eV can be observed or ruled out at 3σ significance.

As an example of the physical implications of these constraints, let us apply to them to the ($s = 3/2$) gravitino, which is related to the scale of SUSY breaking in some models. The gravitino is cosmologically equivalent to the neutrinolike Weyl relic that we have studied, as only the $s = 1/2$ modes are thermalized with the SM plasma in the early Universe [53], and are expected to have the lowest relic temperature of 0.91 K. This has allowed previous work to constrain the gravitino mass by requiring that their abundance does not overcome that of the cosmological dark matter [86]. Our forecast above shows that current data is sensitive to gravitinos heavier than $m_X = 2.85$ eV, which is around the benchmark of some models of SUSY breaking [87,88], and a factor of a few better than the best limits currently available [53,89]. Upcoming data from CMB-S4 combined with Euclid is expected to further detect such gravitino population masses above 0.63 eV. Under the assumption that a cosmological gravitino population no longer exchanges entropy after decoupling from the SM bath, we can relate constraints on m_X to bounds on the SUSY breaking scale $\Lambda_{\rm SUSY} \sim \sqrt{m_X M_{\rm Pl}}$ [54,90]. Our forecasted Planck and BOSS dataset translates to an upper bound $\Lambda_{\rm SUSY} \lesssim 80$ TeV, whereas the CMB-S4 and Euclid datasets lower this to $\Lambda_{\rm SUSY} \lesssim 50$ TeV. These projections are interestingly complementary to the energy range that will be reached by the proposed $\mathcal{O}(100\ \text{TeV})$ particle collider, showing the promise of our approach.

We also consider a Dirac fermion, with $g_X = 4$ and mass m_X. In terms of the equivalent Weyl fermion, this corresponds to a temperature $T_W^{\rm eq} = 1.08$ K and mass $m_W^{\rm eq} = 1.19 m_X$. In Fig. 8(b), we show that the combined Planck and BOSS datasets are forecasted to observe or rule out such particles above 1.30 (1.12) eV at 3σ significance. For Planck and DESI, the 3σ constraint is lowered to 0.61 (0.52) eV. Interestingly, CMB-S4 data will enable the parameter space of Dirac fermions with any mass to be observed or ruled out at 3σ significance when combined with LSS data from DESI.

2. Bosonic relics

We now move to bosonic degrees of freedom. First, we study a minimum-temperature real scalar, with $s = 0$, $g_X = 1$, and mass m_X. This is equivalent to a Weyl relic with $T_W^{\rm eq} = 0.79$ K and $m_W^{\rm eq} = 1.01 m_X$. We show in

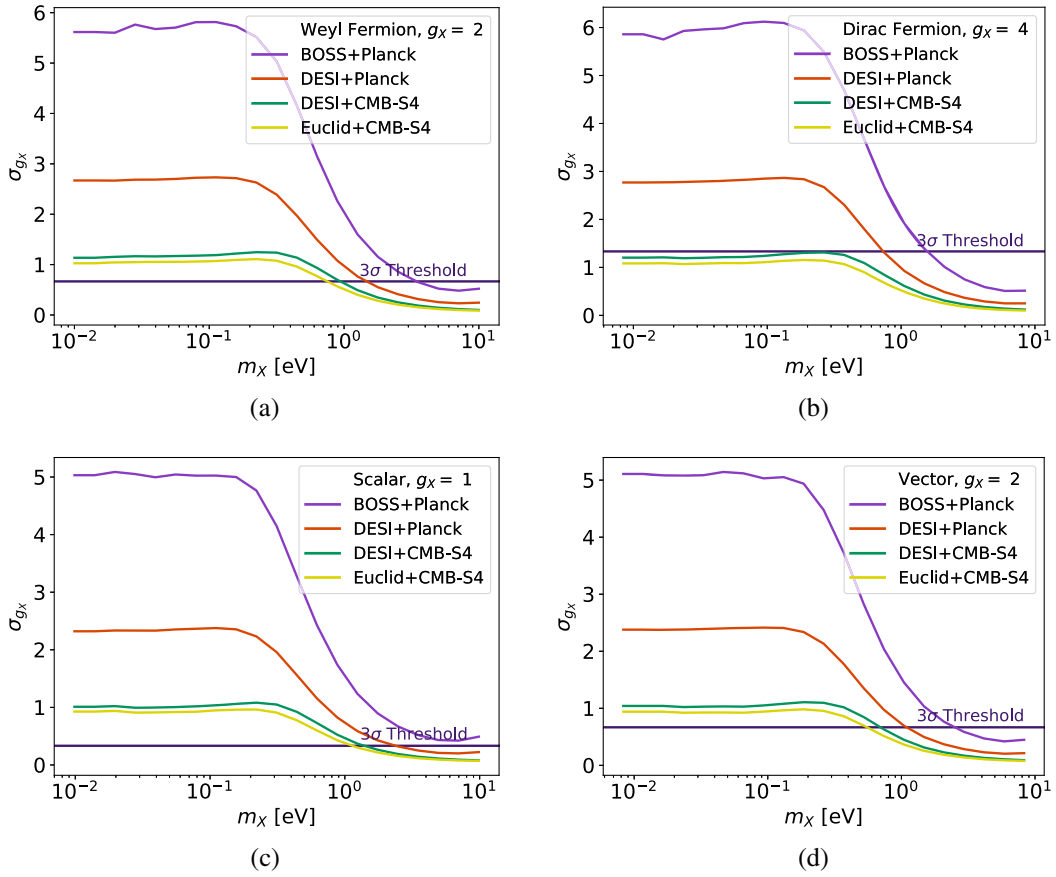

FIG. 8. Forecasted error on the relic degrees of freedom for a neutrinolike Weyl fermion (with fiducial $g_X = 2$, top left), a Dirac fermion ($g_X = 4$, top right), a real scalar ($g_X = 1$, bottom left), and a vector particle ($g_X = 2$, bottom right), all at their minimum temperature $T_X = 0.91$ K, for various combinations of CMB + LSS experiments. The horizontal line denotes the uncertainty required to detect each relic at 3σ.

Fig. 8(c) that, while the combination of presently available Planck and BOSS datasets cannot constrain scalar relics at the 3σ significance, DESI and Planck can jointly rule out scalars with masses above 1.96 (1.61) eV. Further, the combination of CMB-S4 with either the DESI or Euclid datasets can observe or rule out real scalar bosonic relics above 1.14 (1.06) and 0.93 (0.87) eV, respectively.

Second, we consider a massive vector, with $s = 1$ and $g_X = 2$. This massive vector is equivalent to a Weyl relic with $T_W^{\rm eq} = 0.94$ K and $m_W^{\rm eq} = 1.21 m_X$. In Fig. 8(d) we show that the combination of Planck and BOSS datasets can observe or rule out massive vector bosonic relics above 2.05 (1.79) eV, whereas substituting BOSS for DESI improves this number to 0.90 (0.75) eV. Combining the CMB-S4 and Euclid datasets further improves this to 0.47 (0.44) eV.

C. Neutrino-mass forecasts

We have detailed in each previous subsection the constraints with and without marginalizing over neutrino masses to emphasize the importance of this step, as it is seen to affect results noticeably when LSS information is being considered. We note that DESI is particularly sensitive to the marginalization or fixing of $\sum m_\nu$. This is due to its chosen bias prescription, which does not include a parameter to marginalize over the redshift dependence of the bias, as opposed to BOSS and Euclid. This underscores the sensitivity of our results to the details of the bias prescription, which is further explored in our companion paper [48].

As a consequence of our analysis, we can also forecast how much neutrino-mass measurements would be affected

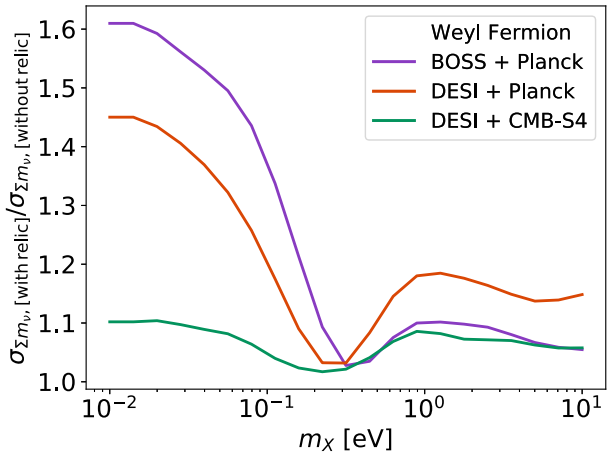

FIG. 9. Forecasted DESI + CMB-S4 uncertainty on the sum $\sum m_\nu$ of neutrino masses, when it is jointly searched for with a relic of mass m_X and temperature $T_X = 0.91$ K. The degeneracy is minimized at $\sim\mathcal{O}(0.3$ eV) for all particle types, although the constraints on neutrino masses using CMB data from Planck are always expected to weaken by ~10%, if a new light relic is present.

by the presence of a LIMR, given the degeneracies between $\sum m_\nu$ and g_X shown in Fig. 3. We show in Fig. 9 the relative increment in the error of the sum $\sum m_\nu$ of neutrino masses when marginalizing over a relic of varying mass. For reference, we forecast $\sigma(\sum m_\nu)$ to be 61.1×10^{-3} eV for BOSS and Planck, 28.2×10^{-3} eV for DESI and Planck, and 24.1×10^{-3} eV for DESI and CMB-S4, with a fiducial at the (normal-hierarchy) minimum $\sum m_\nu = 60 \times 10^{-3}$ eV and no other relics. The degradation in the expected errors ranges from 10% for heavy relics and futuristic data (DESI+S4), to nearly 100% for lower masses and current or upcoming data (BOSS/DESI+Planck). Note that for relics of $m_X \approx 0.3$ eV the degradation minimizes in all survey specifications. This mass corresponds to relics that become non-relativistic around the time of recombination. In essence, heavier relics produce suppression in the matter fluctuations, whereas lighter relics chiefly affect CMB and LSS observables through their change in $N_{\rm eff}$. We encourage the reader to see our companion paper [48] for in-depth neutrino forecasts without relics.

V. CONCLUSIONS

In this work we have studied how well current and upcoming cosmological surveys can detect LIMRs, focusing on the $10^{-2} - 10^{1}$ eV mass range. These particles become nonrelativistic before $z = 0$, and thus affect the formation of structures in the Universe. By combining information from the CMB and the LSS we have shown that a large swath of the 2D-parameter space (of relic mass and temperature) will be probed by upcoming surveys.

There is a minimum temperature that any relic that was in thermal equilibrium with the Standard Model should have, $T_X^{(0)} = 0.91$ K. Interestingly, we find that Weyl, vectors, and Dirac relics with this temperature, and masses above ≈1 eV, can be observed or ruled out at the 3σ significance using the presently available combination of Planck and BOSS datasets. Looking slightly to the future, the Planck and DESI datasets will improve these constraints, and reduce the minimum mass allowed for LIMRs by roughly 50%. The more futuristic Euclid and CMB-S4 datasets will present an 80% improvement and, in the case of Dirac fermions, fully cover the parameter space. If the sum of neutrino masses, $\sum m_\nu$, can be learned independently of CMB and LSS surveys, the effect of fixing the $\sum m_\nu$ parameter manifests as an approximate 20% improvement on these constraints. This could be accomplished, for example, by KATRIN which currently sets the leading upper bound on the effective electron neutrino mass of 1.1 eV, independently of cosmology [91]. We emphasize that the effect of marginalizing $\sum m_\nu$ significantly weakens the 3σ constraints for some of the cases reported, suggesting that it is important to account for $\sum m_\nu$ in any search for LIMRs. While the need to properly account for $\sum m_\nu$ has been discussed in previous work

[17,27,39,92–94], our analysis, which does so for massive but light relics, is unprecedented.

This result is particularly interesting for the case of the gravitino. Since the gravitino would have a cosmological imprint identical to a Weyl fermion, we have shown that Planck and BOSS can observe or rule out gravitinos heavier than 2.85 eV. If a gravitino, or any other LIMR, were detected, then their parameters (i.e., mass and temperature) could also be measured, as suggested in Ref. [25].

In summary, while light relics are commonly assumed to be nearly massless—and constrained through $N_{\rm eff}$—here we have shown that relics with masses on the $10^{-2} - 10^{1}$ eV scale can be constrained with cosmological data. These constraints are broadly expected to apply to the full range of allowed relic masses, from effectively massless to saturating the DM abundance. This complements current efforts in the search of relics, allowing many new routes for finding physics beyond the Standard Model.

ACKNOWLEDGMENTS

We thank Sunny Vagnozzi for insightful comments on a previous version of this manuscript. We also thank Prateek Agrawal and David Pinner for discussions. N. D. was supported by a National Physical Science Consortium Graduate Fellowship for STEM Diversity. C. D. and J. B. M. were partially supported by NSF Grant No. AST-1813694.

APPENDIX A: MCMC VALIDATION OF FISHER FORECASTS

In this Appendix we show a comparison of our Fisher formalism and an MCMC analysis of the same mock data to confirm our Fisher analysis throughout the main text. In Fig. 10 we show the MCMC (solid) and Fisher forecasted (dotted) marginalized posteriors for cosmological parameters and nuisance parameters (including the neutrino mass $\sum m_\nu$), assuming CMB-S4 + DESI data. This figure shows that the predicted errors agree remarkably well between our Fisher-matrix approach and the full MCMC of mock data.

Moreover, we show posteriors for models with and without the growth induced scale-dependent modification to the bias (as described in our companion paper [48]), which we termed GISDB. The MCMC results are from Ref. [48], and the Fishers are calculated here. The non-GISDB Fisher ellipses are centered on the corresponding MCMC maximum likelihood point. The GISDB ones, however, are shifted by [95]

$$\delta\theta_i = (F^{-1})_{ij} D_j, \tag{A1}$$

in each parameter θ_i, where we have defined

$$D_j = \sum_z \int k^2 \mathrm{d}k \int \mathrm{d}\mu \frac{V(z)}{2(2\pi)^2} \left(\frac{\partial \log \tilde{P}_g(k,\mu)}{\partial \theta_j}\right) \times (\tilde{P}_{g,\rm GISDB}(k,\mu) - \tilde{P}_{g,\rm no\ GISDB}(k,\mu)) \left(\frac{\bar{n}\tilde{P}_g}{\bar{n}\tilde{P}_g + 1}\right)^2, \tag{A2}$$

and the GISDB Fisher ellipses are computed centered on the shifted best fit. As shown, the good cohesion between the Fisher and MCMC analyses of the data, particularly in the inclusion of the GISDB effect, demonstrates that the considered effects are well-approximated by the linearity of the Fisher approach, and thus validates the constraints we present on additional light relics.

APPENDIX B: MARGINALIZATION OVER THE RELIC MASS

Throughout the main text, the LIMR mass has been held fixed. In this Appendix, we allow the LIMR mass to vary in the forecasts to study what effect this has on the LIMR constraints presented earlier, as well as to study how well a prospective LIMR detection could constrain its properties.

For all combinations of LIMR species, galaxy surveys and CMB experiments studied in this work, we find that marginalizing over the LIMR mass m_X weakens the constraint on the relic degrees of freedom g_X, as expected. This effect is most exaggerated in the cases where the constraint is dominantly set by LSS information. In a joint Planck-BOSS analysis, high-mass relics (with $m_X \geq 0.2$ eV) see the g_X constraint weakened by nearly a factor of 2. In cases where CMB information dominates, however, such as when adding CMB-S4 to BOSS, the g_X constraint is weakened by no more than 6%. Adding Planck information to DESI, the higher-mass region sees the g_X constraint weakened by no more than a factor of 2. Adding CMB-S4 to DESI, the g_X constraint is weakened by no more than 25%.

In Figs. 11 and 12, we illustrate this effect, assuming that a Weyl fermion with fiducial $T_X = 0.91$ K and different values of m_X is observed using different combinations of galaxy and CMB surveys. The broadening of the error bars is primarily driven by the LSS information and, as a consequence, the biggest shift in constraints is observed for datasets that are primarily or exclusively constrained by the galaxy surveys.

We see in Fig. 11 that the Planck constraint monotonically weakens with increasing fiducial relic mass. This can be explained by the decreasing effect of a relic on the radiation energy density ρ_r which the CMB is primarily sensitive to. At low masses, the Planck dataset demonstrates an orthogonal relationship between the relic mass and degrees of freedom. Considering that at low masses, changes in mass will modify the weak lensing signal of the CMB and produce no change in ρ_r yet small changes in g_X

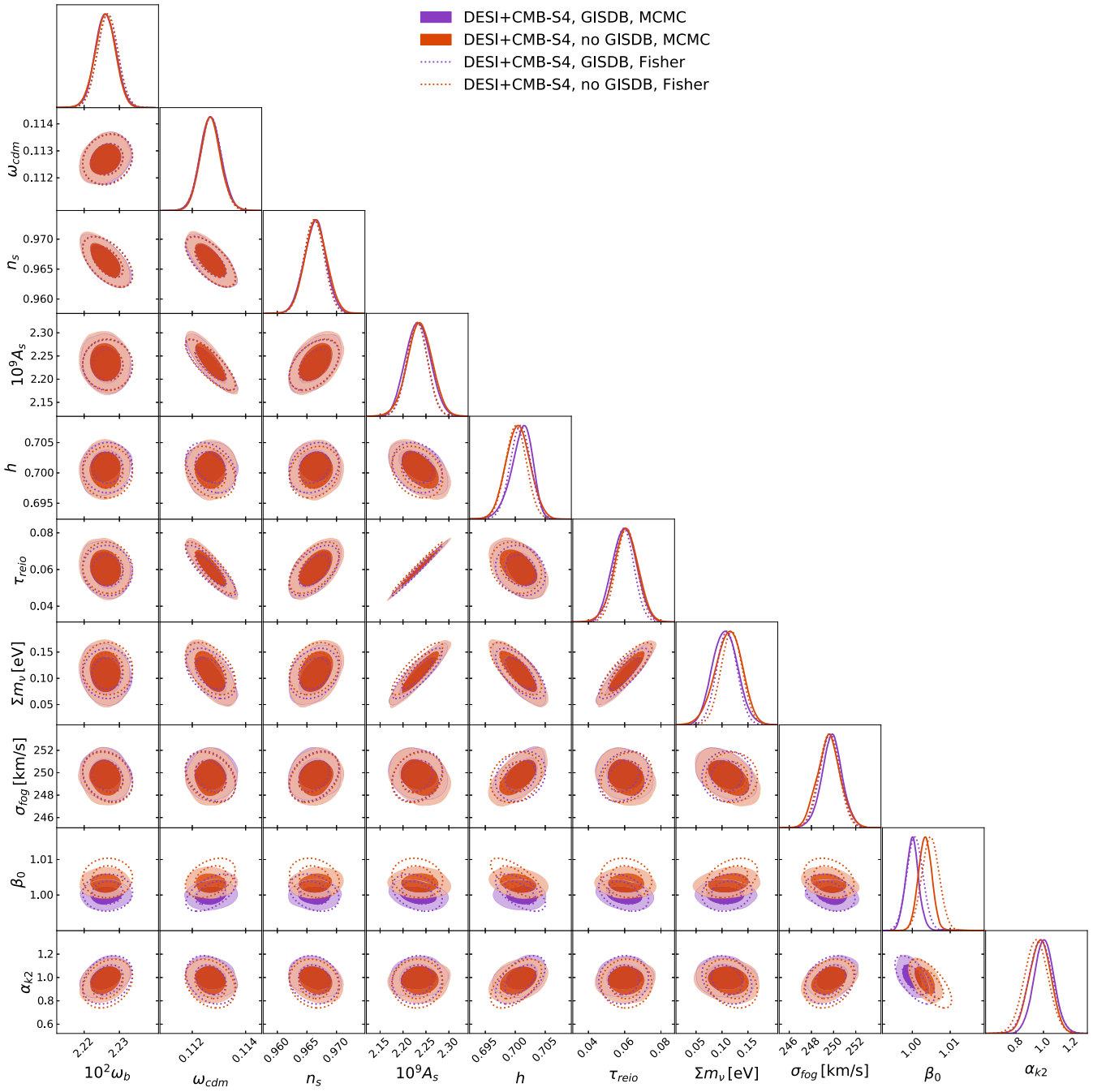

FIG. 10. MCMC and Fisher forecasted marginalized posteriors for cosmological parameters and nuisance parameters for a joint DESI + CMB-S4 analysis. The degenerate hierarchy is assumed with a total mass of $\sum m_\nu = 0.1$ eV. Models with and without the bias step (GISDB) are considered. As shown, the good consistency between MCMC and Fisher results, particularly the reproduced shift in parameters upon turning off GISDB, demonstrates that the effects we consider are well-captured at linear order and validates our results regarding the detectability of LIMRs.

will produce directly proportional changes in ρ_r we expect a nearly orthogonal relationship between these two parameters at low masses primarily governed by Eq. (4), as the CMB signal is dominated by changes to ρ_r. However, as the fiducial relic mass is increased, and the relic effect on ρ_r at recombination becomes smaller, the CMB becomes sensitive to the relic primarily through its effect on the weak lensing signal and the governing relationship changes to Eq. (6) which is directly proportional to the product of m_X and g_X. Thus, these two parameters are expected to develop an anticorrelation at high masses in the CMB dataset, which is indeed what we observe in Fig. 11 at higher masses.

Now we consider how the degeneracy direction in the $m_X - g_X$ plane varies at different relic masses for the LSS

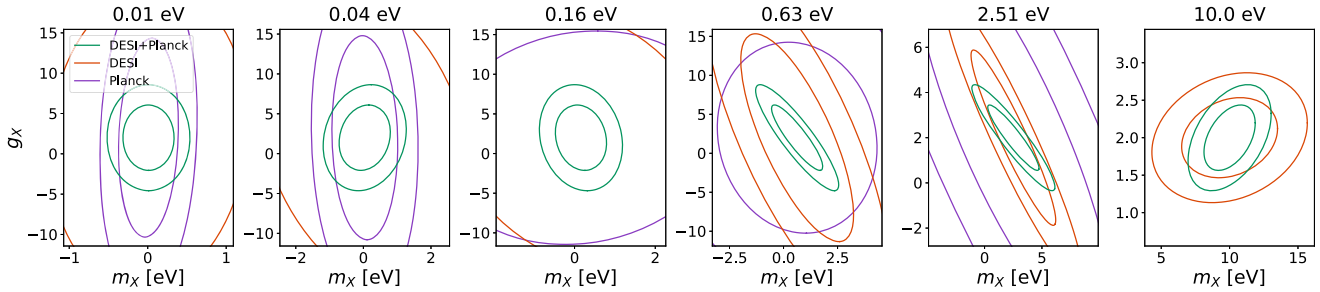

FIG. 11. Fisher-matrix forecasted marginalized posteriors for the parameters g_X and m_X. In this forecast, the LIMR mass has been allowed to vary in addition to its degrees of freedom. We present the marginalized posterior contours for five choices of the fiducial LiMR mass: 10^{-2}, $10^{-1.4}$, $10^{-0.8}$, $10^{-0.2}$, $10^{0.4}$, and 10^{1} eV. As shown, the degeneracy lines are driven by the relative orthogonality of CMB information at low masses, and by strong degeneracy in the LSS data at intermediate to high masses.

datasets. Here the scales affected by the relic, as governed by Eq. (5), and by the magnitude of the effect, as determined by Eq. (6), control the effect on the LSS signal. At low masses, the contribution of the relic to ω_M is small and the relic will primarily affect the LSS signal through its free-streaming scale, which is independent of g_X. So at small relic masses, we expect m_X and g_X to be approximately orthogonal. As the fiducial relic mass is increased, the contribution of the relic to P_M and hence to the LSS signal increases and is again proportional to the product of m_X and g_X. So with increasing relic mass, we generally expect an anticorrelation to develop between the relic mass and degrees of freedom. We again see this to be the case in Fig. 11.

As discussed above, allowing the relic mass to vary modifies the constraints of the LSS and CMB datasets such that the accuracy of those constraints is generally less affected for lower mass relics. As the relic occupies a greater portion of Ω_M, it becomes more important to simultaneously vary the relic mass and degrees of freedom. We emphasize that for a fixed relic abundance, there is a degeneracy between the relic parameters m_X, T_X, g_X according to Eq. (6). This allows us to translate constraints on any two of these parameters into constraints on the third parameter. Where we have allowed the relic mass and degrees of freedom to vary, the resulting constraints can be translated to errors on the temperature. We also bring attention to the fact that marginalizing over the relic mass is only valid in the neighborhood of parameter space around each fiducial choice, and not over the entire parameter space of masses permitted.

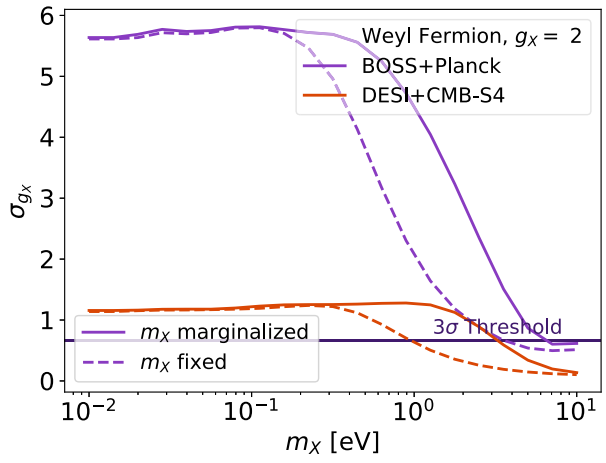

FIG. 12. Forecasted sensitivity on the relic degrees of freedom g_X for a Weyl fermion with (solid) and without (dashed) marginalization over relic mass m_X for combinations of datasets BOSS + Planck and DESI + CMB-S4. As expected, there is little degeneracy in the low-mass limit, where the relic mainly contributes as $N_{\rm eff}$; the $g_X - m_X$ degeneracy enters most at intermediate masses.

APPENDIX C: SAMPLING OF FULL MODEL POSTERIOR FORECASTS

Datasets with different parameter degeneracies can powerfully constrain parameters when combined. To illustrate this complementary effect between CMB and LSS surveys, we present a sampling of fully marginalized posteriors in Fig. 13 for a Weyl (neutrinolike) relic with temperature 0.91 K and mass 0.01 eV. In each figure, we present constraints using only DESI (red), only Planck (violet), and the joint dataset (green).

As in the case of the LIMR parameter g_X (number of degrees of freedom) discussed in the main text, the addition of LSS information to CMB data will generally break degeneracies between parameters. As an interesting example, we observe that the LSS provides a measurement of $\omega_{\rm cdm}$ that is very close to orthogonal from the CMB one, breaking degeneracies with A_s, n_s, and g_X for very light relic masses. DESI information also serves to set the measurements on h and $\sum m_\nu$, which are poorly measured by Planck as their effects on the CMB are degenerate. In turn, the LSS by itself is generally ineffective at measuring the other cosmological parameters, and provides no information on $\tau_{\rm reio}$. While, as illustrated in Fig. 3, the degeneracies between g_X and other parameters shift significantly between relics of different masses, those between the cosmological parameters themselves remain largely unchanged.

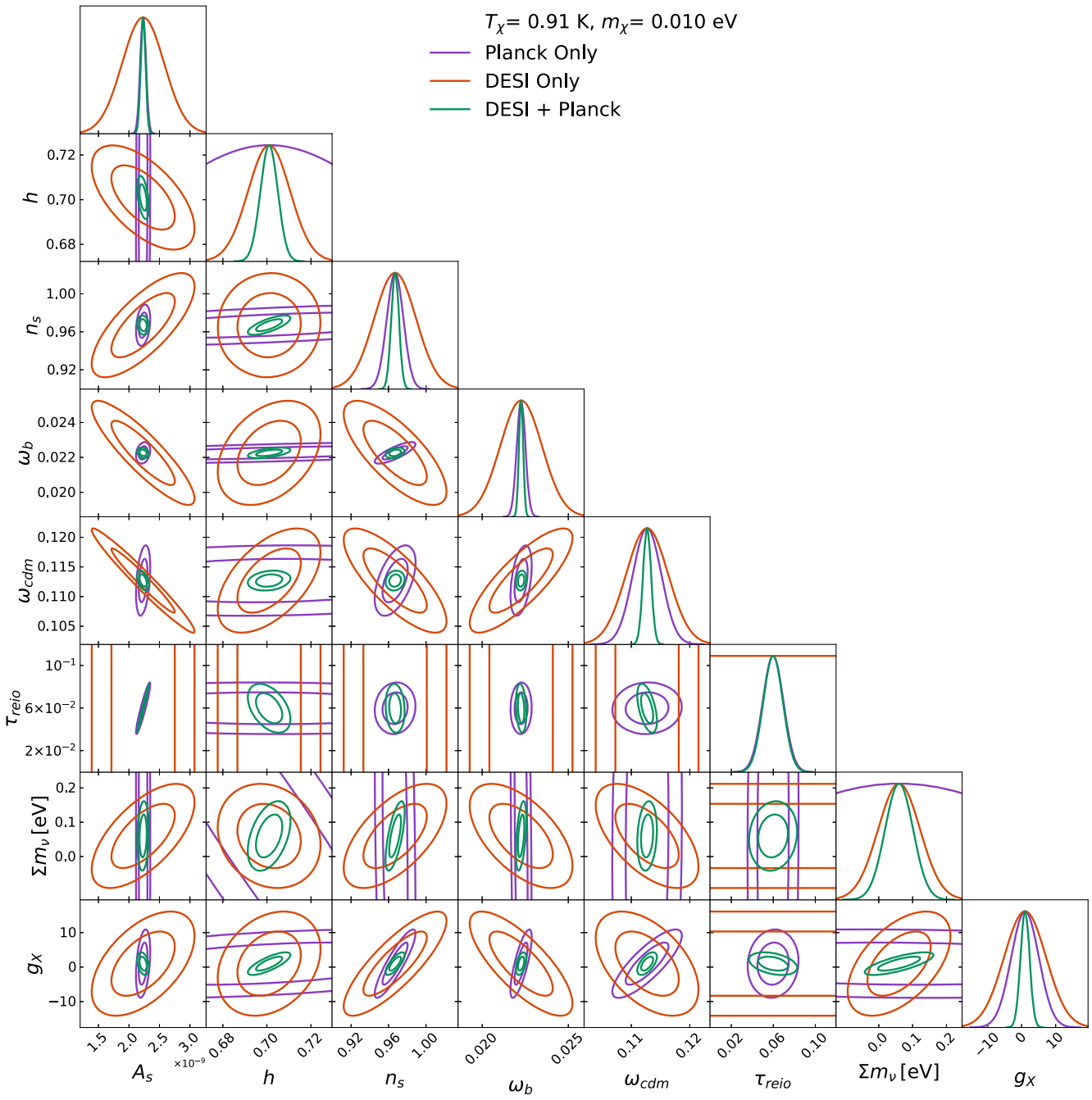

FIG. 13. Two-dimensional posterior distributions for parameter forecasts using DESI + Planck, and each experiment individually. We assume here the presence of a Weyl fermion LIMR ($g_X = 2$) with $T_X = 0.91$ K and $m_X = 0.01$ eV. As shown, the complementarity between the two datasets results in marked improvement on the sensitivity to such a relic.

[1] R. Peccei and H. R. Quinn, Phys. Rev. Lett. **38**, 1440 (1977).
[2] D. H. Weinberg, J. S. Bullock, F. Governato, R. Kuzio de Naray, and A. H. G. Peter, Proc. Natl. Acad. Sci. U.S.A. **112**, 12249 (2015).
[3] P. Svrcek and E. Witten, J. High Energy Phys. 06 (2006) 051.
[4] A. Arvanitaki, S. Dimopoulos, S. Dubovsky, N. Kaloper, and J. March-Russell, Phys. Rev. D **81**, 123530 (2010).

[5] S. Abel, M. Goodsell, J. Jaeckel, V. Khoze, and A. Ringwald, J. High Energy Phys. 07 (2008) 124.
[6] T. Beranek, H. Merkel, and M. Vanderhaeghen, Phys. Rev. D **88**, 015032 (2013).
[7] N. Arkani-Hamed and N. Weiner, J. High Energy Phys. 12 (2008) 104.
[8] R. Essig, P. Schuster, and N. Toro, Phys. Rev. D **80**, 015003 (2009).
[9] K. Cheung and T.-C. Yuan, J. High Energy Phys. 03 (2007) 120.
[10] H. Goldberg and L. J. Hall, Phys. Lett. B **174**, 151 (1986).
[11] D. Feldman, Z. Liu, and P. Nath, Phys. Rev. D **75**, 115001 (2007).
[12] S. Fukuda *et al.* (Super-Kamiokande Collaboration), Phys. Rev. Lett. **85**, 3999 (2000).
[13] G. Mention, M. Fechner, T. Lasserre, T. A. Mueller, D. Lhuillier, M. Cribier, and A. Letourneau, Phys. Rev. D **83**, 073006 (2011).
[14] A. A. Aguilar-Arevalo *et al.* (MiniBooNE Collaboration), Phys. Rev. Lett. **110**, 161801 (2013).
[15] M. Dentler, A. Hernández-Cabezudo, J. Kopp, P. A. N. Machado, M. Maltoni, I. Martinez-Soler, and T. Schwetz, J. High Energy Phys. 08 (2018) 010.
[16] K. Benakli, Y. Chen, E. Dudas, and Y. Mambrini, Phys. Rev. D **95**, 095002 (2017).
[17] S. Bashinsky and U. Seljak, Phys. Rev. D **69**, 083002 (2004).
[18] Z. Hou, R. Keisler, L. Knox, M. Millea, and C. Reichardt, Phys. Rev. D **87**, 083008 (2013).
[19] D. Baumann, D. Green, J. Meyers, and B. Wallisch, J. Cosmol. Astropart. Phys. 01 (2016) 007.
[20] G. Mangano, G. Miele, S. Pastor, T. Pinto, O. Pisanti, and P. D. Serpico, Nucl. Phys. **B729**, 221 (2005).
[21] P. F. de Salas and S. Pastor, J. Cosmol. Astropart. Phys. 07 (2016) 051.
[22] K. Akita and M. Yamaguchi, J. Cosmol. Astropart. Phys. 08 (2020) 012.
[23] N. Aghanim *et al.* (Planck Collaboration), Astron. Astrophys. **641**, A6 (2020).
[24] A. Boyarsky, J. Lesgourgues, O. Ruchayskiy, and M. Viel, J. Cosmol. Astropart. Phys. 05 (2009) 012.
[25] A. Banerjee, B. Jain, N. Dalal, and J. Shelton, J. Cosmol. Astropart. Phys. 01 (2018) 022.
[26] J. Baur, N. Palanque-Delabrouille, C. Yèche, A. Boyarsky, O. Ruchayskiy, E. Armengaud, and J. Lesgourgues, J. Cosmol. Astropart. Phys. 12 (2017) 013.
[27] S. Dodelson, K. Heitmann, C. Hirata, K. Honscheid, A. Roodman, U. Seljak, A. Slosar, and M. Trodden, arXiv: 1604.07626.
[28] D. Baumann, D. Green, and M. Zaldarriaga, J. Cosmol. Astropart. Phys. 11 (2017) 007.
[29] C. Brust, D. E. Kaplan, and M. T. Walters, J. High Energy Phys. 12 (2013) 058.
[30] K. N. Abazajian *et al.* (CMB-S4 Collaboration), arXiv: 1610.02743.
[31] R. H. Cyburt, B. D. Fields, K. A. Olive, and T.-H. Yeh, Rev. Mod. Phys. **88**, 015004 (2016).
[32] C. Cheung, G. Elor, and L. Hall, Phys. Rev. D **84**, 115021 (2011).
[33] C. Dvorkin, T. Lin, and K. Schutz, Phys. Rev. D **99**, 115009 (2019).
[34] B. D. Fields, K. A. Olive, T.-H. Yeh, and C. Young, J. Cosmol. Astropart. Phys. 03 (2020) 010.
[35] G. Rossi, C. Yèche, N. Palanque-Delabrouille, and J. Lesgourgues, Phys. Rev. D **92**, 063505 (2015).
[36] N. Palanque-Delabrouille *et al.*, J. Cosmol. Astropart. Phys. 11 (2015) 011.
[37] S. Alam *et al.* (BOSS Collaboration), Mon. Not. R. Astron. Soc. **470**, 2617 (2017).
[38] P. Zarrouk *et al.*, Mon. Not. R. Astron. Soc. **477**, 1639 (2018).
[39] D. Baumann, D. Green, and B. Wallisch, J. Cosmol. Astropart. Phys. 08 (2018) 029.
[40] Y. Ali-Haimoud and S. Bird, Mon. Not. R. Astron. Soc. **428**, 3375 (2012).
[41] S. Bird, Y. Ali-Haïmoud, Y. Feng, and J. Liu, Mon. Not. R. Astron. Soc. **481**, 1486 (2018).
[42] J. Lesgourgues and S. Pastor, Phys. Rep. **429**, 307 (2006).
[43] D. Blas, J. Lesgourgues, and T. Tram, J. Cosmol. Astropart. Phys. 07 (2011) 034.
[44] M. LoVerde and M. Zaldarriaga, Phys. Rev. D **89**, 063502 (2014).
[45] M. LoVerde, Phys. Rev. D **90**, 083530 (2014).
[46] J. B. Muñoz and C. Dvorkin, Phys. Rev. D **98**, 043503 (2018).
[47] C.-T. Chiang, M. LoVerde, and F. Villaescusa-Navarro, Phys. Rev. Lett. **122**, 041302 (2019).
[48] W. L. Xu, N. DePorzio, J. B. Muñoz, and C. Dvorkin, preceding paper, Phys. Rev. D **103**, 023503 (2021).
[49] P. J. E. Peebles, Astrophys. J. **146**, 542 (1966).
[50] D. A. Dicus, E. W. Kolb, A. M. Gleeson, E. C. G. Sudarshan, V. L. Teplitz, and M. S. Turner, Phys. Rev. D **26**, 2694 (1982).
[51] S. Bashinsky and U. C. V. Seljak, Phys. Rev. D **69**, 083002 (2004).
[52] Z. Hou, R. Keisler, L. Knox, M. Millea, and C. Reichardt, Phys. Rev. D **87**, 083008 (2013).
[53] K. Osato, T. Sekiguchi, M. Shirasaki, A. Kamada, and N. Yoshida, J. Cosmol. Astropart. Phys. 06 (2016) 004.
[54] S. P. Martin, A Supersymmetry primer, in *Perspectives on Supersymmetry*, Vol. 21, edited by G. L. Kane (World Scientific, River Edge, New Jersey, 2010), pp. 1–153.
[55] L. Covi, J. E. Kim, and L. Roszkowski, Phys. Rev. Lett. **82**, 4180 (1999).
[56] M. Reece, J. High Energy Phys. 07 (2019) 181.
[57] K. Abazajian *et al.*, Bull. Am. Astron. Soc. **51**, 209 (2019).
[58] K. S. Dawson, D. J. Schlegel, C. P. Ahn, S. F. Anderson, E. Aubourg, S. Bailey, R. H. Barkhouser, J. E. Bautista, A. Beifiori, A. A. Berlind *et al.*, Astron. J. **145**, 10 (2012).
[59] A. Aghamousa *et al.* (DESI Collaboration), arXiv:1611 .00036.
[60] L. Amendola *et al.*, Living Rev. Relativity **21**, 2 (2018).
[61] M. Archidiacono, S. Hannestad, and J. Lesgourgues, J. Cosmol. Astropart. Phys. 09 (2020) 021.
[62] C. M. Hirata and U. Seljak, Phys. Rev. D **68**, 083002 (2003).
[63] T. Okamoto and W. Hu, Phys. Rev. D **67**, 083002 (2003).
[64] v. Ivezić *et al.* (LSST Collaboration), Astrophys. J. **873**, 111 (2019).

[65] T. Abbott *et al.* (DES Collaboration), arXiv:astro-ph/0510346.
[66] A. Boyle and E. Komatsu, J. Cosmol. Astropart. Phys. 03 (2018) 035.
[67] A. Font-Ribera, P. McDonald, N. Mostek, B. A. Reid, H.-J. Seo, and A. Slosar, J. Cosmol. Astropart. Phys. 05 (2014) 023.
[68] C. Modi, E. Castorina, and U. Seljak, Mon. Not. R. Astron. Soc. **472**, 3959 (2017).
[69] T. Sprenger, M. Archidiacono, T. Brinckmann, S. Clesse, and J. Lesgourgues, J. Cosmol. Astropart. Phys. 02 (2019) 047.
[70] M. Kamionkowski, A. Kosowsky, and A. Stebbins, Phys. Rev. D **55**, 7368 (1997).
[71] M. Zaldarriaga and U. Seljak, Phys. Rev. D **55**, 1830 (1997).
[72] M. Tegmark, Phys. Rev. Lett. **79**, 3806 (1997).
[73] J. B. Muñoz, E. D. Kovetz, A. Raccanelli, M. Kamionkowski, and J. Silk, J. Cosmol. Astropart. Phys. 05 (2017) 032.
[74] S. Galli, K. Benabed, F. Bouchet, J.-F. Cardoso, F. Elsner, E. Hivon, A. Mangilli, S. Prunet, and B. Wandelt, Phys. Rev. D **90**, 063504 (2014).
[75] N. Kaiser, Mon. Not. R. Astron. Soc. **227**, 1 (1987).
[76] P. Bull, P. G. Ferreira, P. Patel, and M. G. Santos, Astrophys. J. **803**, 21 (2015).
[77] E. V. Linder, Phys. Rev. D **72**, 043529 (2005).
[78] I. Zehavi *et al.* (SDSS Collaboration), Astrophys. J. **571**, 172 (2002).
[79] C. Alcock and B. Paczynski, Nature (London) **281**, 358 (1979).
[80] M. Asgari, A. Taylor, B. Joachimi, and T. D. Kitching, Mon. Not. R. Astron. Soc. **479**, 454 (2018).
[81] P. Lemos, A. Challinor, and G. Efstathiou, J. Cosmol. Astropart. Phys. 05 (2017) 014.
[82] A. Moradinezhad Dizgah, H. Lee, J. B. Muñoz, and C. Dvorkin, J. Cosmol. Astropart. Phys. 05 (2018) 013.
[83] A. R. Cooray, Mon. Not. R. Astron. Soc. **348**, 250 (2004).
[84] C. Hahn, F. Beutler, M. Sinha, A. Berlind, S. Ho, and D. W. Hogg, Mon. Not. R. Astron. Soc. **485**, 2956 (2019).
[85] P. Larsen, A. Challinor, B. D. Sherwin, and D. Mak, Phys. Rev. Lett. **117**, 151102 (2016).
[86] T. Moroi, H. Murayama, and M. Yamaguchi, Phys. Lett. B **303**, 289 (1993).
[87] A. Hook and H. Murayama, Phys. Rev. D **92**, 015004 (2015).
[88] A. Hook, R. McGehee, and H. Murayama, Phys. Rev. D **98**, 115036 (2018).
[89] M. Viel, J. Lesgourgues, M. G. Haehnelt, S. Matarrese, and A. Riotto, Phys. Rev. D **71**, 063534 (2005).
[90] S. Deser and B. Zumino, Phys. Rev. Lett. **38**, 1433 (1977).
[91] M. Aker *et al.* (KATRIN Collaboration), Phys. Rev. Lett. **123**, 221802 (2019).
[92] D. D. Baumann, F. Beutler, R. Flauger, D. R. Green, A. z. Slosar, M. Vargas-Magaña, B. Wallisch, and C. Yèche, Nat. Phys. **15**, 465 (2019).
[93] D. Green *et al.*, Bull. Am. Astron. Soc. **51**, 159 (2019), https://baas.aas.org/pub/2020n3i159.
[94] A. Font-Ribera, P. McDonald, N. Mostek, B. A. Reid, H.-J. Seo, and A. Slosar, J. Cosmol. Astropart. Phys. 05 (2014) 023.
[95] J. B. Muñoz, D. Grin, L. Dai, M. Kamionkowski, and E. D. Kovetz, Phys. Rev. D **93**, 043008 (2016).